


Trapping and scattering of a multiflagellated bacterium by a hard surface

Alexander P. Petroff  and Schuyler McDonough

Department of Physics, Clark University, Worcester, Massachusetts 01610, USA



(Received 19 June 2023; accepted 25 January 2024; published 1 March 2024)

Thiovulum majus, which is one of the fastest known bacteria, swims using hundreds of flagella. Unlike typical pusher cells, which swim in circular paths over hard surfaces, *T. majus* localize near hard boundaries by turning their flagella to exert a net force normal to the surface. To probe the torques that stabilize this hydrodynamically bound state, the trajectories of several thousand collisions between a *T. majus* cell and a wall of a quasi-two-dimensional microfluidic chamber are analyzed. Measuring the fraction of cells escaping the wall either to the left or to the right of the point of contact—and how this probability varies with incident angle and time spent in contact with the surface—maps the scattering dynamics onto a first passage problem. These measurements are compared to the prediction of a Fokker-Planck equation to fit the angular velocity of a cell in contact with a hard surface. This analysis reveals a bound state with a narrow basin of attraction in which cells orient their flagella normal to the surface. The escape angle predicted by matching these near field dynamics with the far-field hydrodynamics is consistent with observation. We discuss the significance of these results for the ecology of *T. majus* and their self-organization into active chiral crystals.

DOI: [10.1103/PhysRevE.109.034403](https://doi.org/10.1103/PhysRevE.109.034403)

I. INTRODUCTION

Microbes in their natural environments often live in close proximity to surfaces such as the air-water interface, sediment grains in water-saturated soils, and sinking detritus [1–4]. When a cell swims near a surface, the flow it generates is perturbed by the presence of the boundary. The perturbed flow turns and advects the swimming cell [5–9]. Microbes have evolved to exploit these flows to better colonize new environments [10], improve foraging and mating strategies [11], and navigate heterogeneous environments [12–14].

Past work on the hydrodynamic coupling between cells and surfaces has focused on a relatively small number of domesticated species [5], which poorly represent the true diversity of microbial form and locomotion observed in nature [15]. To better understand the effect of more complex flagellation patterns of cell-surface interactions, we study the sediment microbe *Thiovulum majus* [16–19], which is one of the fastest-known bacteria [20]. *Thiovulum majus* uses hundreds of flagella to swim at a speed up to $U \approx 600 \mu\text{m s}^{-1}$ [21] and turn smoothly in chemical gradients [22]. Figure 1(a), which is taken from Ref [16], shows an electron micrograph of a typical cell. The body length of *T. majus* varies considerably between cells from $5 \mu\text{m}$ to $25 \mu\text{m}$ depending on the environment from which the cells are enriched as well as the growth stage of the cell [16]. The cells described here are intermediate in size, having a body length $2a = 12 \pm 2.5 \mu\text{m}$ (standard deviation, SD). The body is a slightly prolate ellipsoid with a typical aspect ratio of about 1.15 [19]. The flagella, which cover the body of the cell, are similar in length to the cell radius [16].

Thiovulum majus cells interact with surfaces in two distinct ways. In nature, these cells attach to detritus by means of a $\sim 100 \mu\text{m}$ -long mucus tether that is extruded from the cell posterior [16]. Once attached, the cell rotates its flagella to

generate a flow that efficiently stirs its chemical environment [23–25]. The mechanics by which a cell exudes and attaches the mucus tether to a surface have not been investigated. The second type of interaction is observed in the laboratory, where cells self-organize on smooth surfaces into two-dimensional active crystals [26,27]. The cells in these active crystals are hydrodynamically bound to the surface by the flows they create, which turn the cell to exert a force normal to the surface [28,29]. This bound state is unusual among bacteria and is thought to require flagella that are shorter than a critical length that is similar to the body size [28]. Similar active crystals are formed by eukaryotes [30]. The first step in the formation of active crystals by *T. majus* have been experimentally investigated only indirectly, from the motion of trapped cells [27].

Here we investigate the collision between a *T. majus* and the wall of a microfluidic chamber. After a collision, a cell remains near the surface for an average trapping time $\langle t \rangle = 0.21 \pm 0.01 \text{ s}$ (95% confidence interval). However, trapping times are widely distributed. In approximately 20% of collisions, the cell is only momentarily ($t \leq 0.05 \text{ s}$) in contact with the surface before escaping back into the bulk fluid. Figure 1(b) and supplemental video SV1.mp4 show one such collision [31]. A similar fraction of collisions result in the trapping of the cell [Fig. 1(c) and supplemental video SV2.mp4 [31]] near the surface for more than 0.5 s and as long as 17 s. These trapped bacteria do not swim along the circular paths that are typical of pusher cells [5]. Rather, these cells seem to be in a hydrodynamic bound state to the surface [26–29].

As shown in Fig. 2, we observe striking simplicity in the trajectories of escaping cells. The magnitude of the escape angles varies little with incident angle [Fig. 2(a)] and time [Fig. 2(b)]. The distribution of trapping times is shown in Fig. 2(c). Although the distribution of incident angles is widely distributed [Fig. 2(d)], escape angles are narrowly

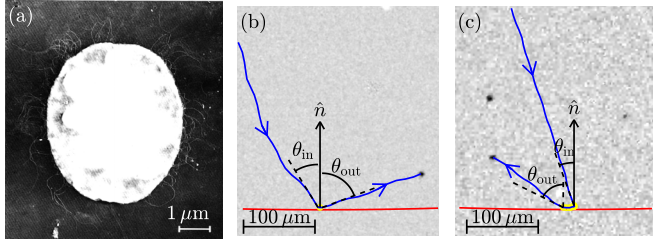


FIG. 1. When a *T. majus* cell collides with a hard wall it may become trapped by the surface. (a) Electron micrograph of a representative cell. The flagella appear as short white lines surrounding the slightly prolate cell body. This image is slightly modified from Ref. [16]. (b) A cell is only momentarily in contact with the surface (yellow dot). The blue line shows the trajectory of the cell with arrows indicating the direction of motion. The incident angle θ_{in} and escape angle θ_{out} are measured from the surface normal \hat{n} . The coordinate system is chosen such that $\theta_{\text{in}} > 0$ for all collisions. $\theta_{\text{out}} > 0$ if the sign of the tangential velocity does not change. (b) A trapped cell may remain in contact with the surface for several seconds. In this example $\theta_{\text{out}} < 0$.

distributed (Fig. 2(e)). Cells that are in fleeting ($t < 0.1$ s) contact with the surface tend to escape at an average angle of $69.2^\circ \pm 0.4^\circ$ (95% confidence interval). Any such cell that approaches the wall from the left escapes to the right and vice versa. In our coordinate system, these cells escape at an angle $\theta_{\text{out}} > 0$. By contrast, cells that remain in contact with the surface for at least 0.5 s are bimodally distributed, being equally likely to escape at either positive or negative angles with mean $\langle |\theta_{\text{out}}| \rangle = 58.0^\circ \pm 0.5^\circ$ (95% confidence interval).

The bimodality of escape directions develops gradually as a cell remains in contact with surface. We measure the probability P_+ that a cell escapes the surface at an angle $\theta_{\text{out}} > 0$ and calculate the associated binomial entropy $S = -P_+ \log(P_+) - (1 - P_+) \log(1 - P_+)$ of the escape direction. As shown in Fig. 2(f), the information of a cell's trajectory before the collision is gradually lost over the course of half a second.

In this article, we show how this erasure of information can be mapped onto a first passage problem [8,9,32,33] to infer the torques acting on a multiflagellated bacterium that is in contact with a wall. Matching the inferred near-field dynamics with the far-field hydrodynamics of a pusher cell predicts the angle at which cells escape.

II. MATERIALS AND METHODS

A. Enrichment of bacteria

Because there are no known techniques to grow *Thiovulum majus* in pure culture, cells must be enriched from environmental samples using well-established methods [16,19,26,27]. We collect sediment from a shallow tide pool in Little Sippewissett Marsh (41.5762° N, 70.6391° W), which is near Woods Hole, Massachusetts. This sediment is stored in the laboratory in a container covered in 15 cm of natural sea water. After three to five days in the container, the sediment-water interface becomes euxinic, and a *T. majus* veil forms a few millimeters above the sediment [23,34], often between strands of eel grass. Cells are collected from a fresh veil with

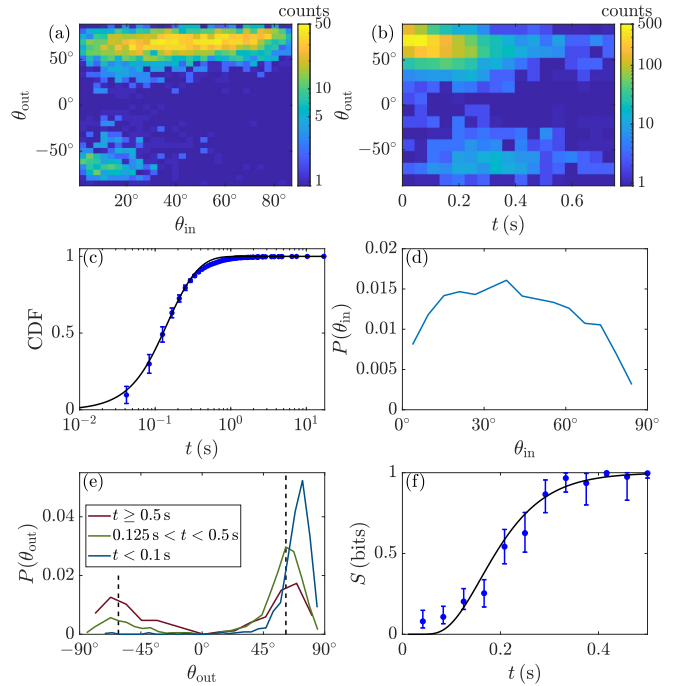


FIG. 2. After a collision, a cell may remain in contact with the surface for several seconds. (a) The magnitude of escape angles θ_{out} varies little with the incident angle θ_{in} . Cells that collide with the surface at small angles are most likely to reverse ($\theta_{\text{out}} < 0$) the tangential component of their motion. (b) Fleeting contact with the surface causes cells to escape at angles $\theta_{\text{out}} > 0$. As cells remain in contact the distribution of escape angles becomes bimodal. (c) The cumulative probability distribution of escape times is compared to the distribution of first passage times calculated from the Fokker-Planck equation [Eq. (3)]. Error bars indicate the 95% confidence intervals. (d) The incident angles θ_{in} are broadly distributed. (e) The probability density function of escape angles is sharply peaked for cells in fleeting contact with the surface. As cells remain in contact with the surface, a symmetric peak emerges. The dashed lines show the prediction of Eq. (6). (f) The binomial entropy S of the escape directions increases continuously as cells remain in contact with the boundary. Error bars indicate the 95% confidence intervals. The black line is equivalent to the fit in Fig. 4(c).

a 1 ml pipette and lightly mixed. After collection the veil reforms, typically within a day.

B. Microfluidic device

Microfluidic chambers—which are produced using standard soft photolithography techniques [35]—are composed of polydimethylsiloxane (PDMS) and sealed on one side by a glass slide. Chambers are quasi-two dimensional, with a height of $150 \mu\text{m}$ and centimeter-scale lateral dimensions. Two similarly designed microfluidic chambers are used in these experiments. In the first set of experiments the shape of the chamber, when viewed from above, is a square ($1 \text{ cm} \times 1 \text{ cm}$). In the second set of experiments [as in Figs. 1(b) and 1(c)], the chamber is circular with a radius of 0.75 cm . We initially suspected that the slight curvature of the wall could lead to measurable differences in the scattering dynamics; however, the statistics presented here were found to be

indistinguishable between the two chamber designs. Because we limit our analysis to the trajectories of cells within $80\ \mu\text{m}$ of a wall, the curvature of a wall is small, being within 1% of flat. Consequently, these measurements are combined in the analysis presented here.

C. Identification and tracking of cells

Thiovulum majus cells are inoculated into the microfluidic chambers described above. The motion of cells as they swim near the outer wall of the chamber is observed using the Zeiss $20\times$ objective, which is focused to a plane $75\ \mu\text{m}$ between the top and bottom of the chamber to limit hydrodynamic interactions between the swimming cell and the chamber.

In each experiment, the motion of cells near one wall of the chamber is recorded at 24 fps using a Nikon D7000 camera. This low temporal resolution likely leads to systematic biases in the measurements of the instantaneous velocity and angular velocity of cells as they approach the boundary. Consequently, we focus our analysis on measurements that can be averaged over several frames. In particular, we focus on the angles at which cells strike the surface and escape from it as well as the time the cell remains in contact with the surface.

Swimming cells appear as dark spots under transmitted light. To identify cells, we first average all frames over the course of a 5 minute experiment. This background image is subtracted from each frame of the video to highlight motion. Swimming cells are identified using an intensity threshold. The threshold value is chosen such that the boundary of the cell identified by the threshold matches visual inspection. Approximating each cell as circular, we record the location and radius a of each cell identified in the frame. The radius of the cells used in our study is $a = 6 \pm 1.25\ \mu\text{m}$ (SD). As cells move slightly in and out of focus, diffraction causes the measured radius of a cell to vary by 8% (SD).

We track the motion of cells swimming within $80\ \mu\text{m}$ of the wall of the chamber. These instantaneous measurements of cell position are connected into trajectories by applying Munkres' Assignment Algorithm. Two representative trajectories are shown as solid blue lines in Figs. 1(b) and 1(c). A small fraction of the trajectories corresponded to cells that are close to division. These cells are atypically large and swim in slightly helical trajectories. To better distinguish torques arising from interactions with the chamber walls from those that are due to the particular flagellation pattern of the cell, these helical trajectories are discarded.

From each triplet of consecutive points in a measured trajectory, we find the distance z between the center of the cell and the nearest point on the wall and the instantaneous velocity \mathbf{v} immediately before and after the cell reached this position. We calculate the instantaneous value of θ and the angular velocity $\partial\theta/\partial t$. Repeating this procedure for each cell yields 13 000 instantaneous measurements of the velocity \mathbf{v} and angular velocity $\partial\theta/\partial t$ for cells at different distances z from the wall, orientations θ , and radii a .

D. Identification and characterization of collisions

Cells are identified as in contact with the surface if the distance between the measured center of the cell and the

chamber wall is less than or equal to the radius of the particular cell, which is measured as the cell approaches the surface. The reliability of this measurement is impaired by the diffraction of light around the cell, which makes it impossible to differentiate between cells that collide with the wall from those that merely approach close to it. Consequently, we focus our analysis on the qualities of the putative collisions that are measured when the cell is separated from the boundary. We measure θ_{in} , θ_{out} , and the time t that the cell is within a cell radius of the wall. As the angles are averaged over several frames, only t is sensitive to our chosen method for identifying contacts. As it is unlikely that a cell remains very close to a surface for extended periods without colliding with it, we expect that it is primarily those cells that briefly approach the boundary that are erroneously identified as making physical contact with it. We return to this point at the end of the Results section. Additionally, the low temporal resolution of these experiments makes it likely that cells that are in contact with the surface for less than the time between frames $0.04\ \text{s}$ are missed entirely.

From each trajectory, we calculate the velocity \mathbf{v} of each cell that collides with the wall of the chamber. To find the incident angle θ_{in} , we measure the incident velocity \mathbf{v}_{in} from the frames immediately before the cell contacts the surface and measure the angle between \mathbf{v}_{in} and the local normal \hat{n} at the point of first contact. Similarly, the asymptotic escape angle θ_{out} is measured relative to the local surface normal at the point where the cell escapes. The velocity of the escaping cell \mathbf{v}_{out} is calculated where hydrodynamic torques are negligible (see Fig. 3). The slight curvature of the circular chamber wall creates an ambiguity in θ_{out} of less than 0.2° , which we ignore.

III. RESULTS

A. Motion of a cell far from a wall

We begin by analyzing a cell's approach to a surface. Figure 3(a) shows that the average angular velocity of cells $\langle\omega\rangle$ decreases with the distance z between the cell and the wall. These data are averaged over all collisions to highlight the tendency of cells to initially approach the wall at a constant angle, $\langle\omega\rangle \approx 0$, and turn parallel to the surface as the distance between the cell and boundary is of the order of the body length.

These dynamics are explained by the far-field hydrodynamics of a pusher cell near a wall [5,36]. At distances $z \gg 2a$, the cell can be approximated as a force dipole. A swimming cell moves as it pushes on the fluid and is advected and rotated by its hydrodynamic image [5,37]. Figure 3(b) shows the dimensionless angular velocity of cells near the boundary. These data are reasonably well fit by the predicted [36] angular velocity of a spherical pusher cell

$$\omega_{\text{far}} = \frac{U}{a} \frac{9\ell a^3}{64z^3} \sin(2\theta), \quad (1)$$

where ℓ is ratio of the dipole length of the cell to its radius and the small angle approximation is made in the comparison to the data. Figure 3(b) shows fair agreement between the theory and observation with a single fit parameter $\ell = 0.78 \pm 0.3$ (95% confidence interval). This value may be slightly biased due to the low temporal resolution of these experiments,

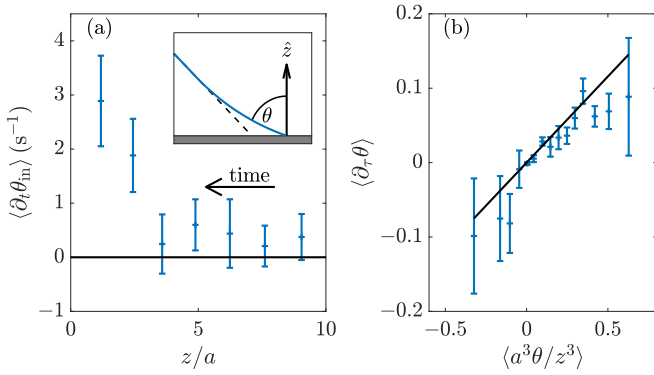


FIG. 3. Cells approaching a wall turn parallel to the surface. (a) The average angular velocity of cells decays with the distance between the cell and the surface. Bars show the 95% confidence interval. Cell rotation is negligible when $z \gg a$. Because these data are average over cells that move towards the surface at different angles, the functional form of this curve depend explicitly on the distribution of incident angles and is shown here only to highlight the sign of the effect. (Inset) Schematic illustrating the trajectory (blue) of a cell as it strikes the wall. The dashed line shows a straight trajectory. (b) The instantaneous rotation of cells near the boundary show a single fixed point $\theta = 0$, which is unstable. To average cells with different sizes and swimming speeds, trajectories are nondimensionalized by each cell's radius a and swimming speed U . Dimensionless time $\tau = Ut/a$. All distances are measured in cell radii a . Only cells that are more than one cell radius from the wall are included in these panels. The black line shows the best linear fit, and the bars indicate the 95% confidence interval.

which affects the measurement of the instantaneous angular velocity. We conclude that these dynamics display a single fixed point at $\theta = 0$, which is unstable.

B. Motion of a cell near a wall

Experiments [26,27] and theory [28,29] show that when a *T. majus* is close to a hard surface, it becomes hydrodynamically bound as it turns its flagella to exert a force normal to the surface. In our notation, $\theta = 0$ is a stable orientation. The stability of this orientation can be understood qualitatively as arising from the flow in the narrow gap between the cell and the surface. Because the velocity gradient in the gap is greater than that between the cell and the bulk fluid, there is a net torque on the cell that causes it to roll until the cell exerts a force normal to the surface [27]. This torque is dominant provided the flagella are sufficiently small compared to the body size [28]. The basin of attraction of this stable orientation was previously estimated to be between 10° and 20° [27]. We speculate that when the cell is turned to an angle greater than θ_b the attraction between the flagella and the surface dominates. It is plausible that this attraction requires a slightly prolate geometry of the cell or the deformation of the flagella [38,39].

This result suggests a simple interpretation of the scattering dynamics. Cells approaching the surface along the surface normal (i.e., $\theta_{\text{in}} \approx 0$) collide with orientations that are within the basin of attraction of the hydrodynamically bound state. These cells localize near the surface until they are freed by

rotational diffusion. By symmetry, a hydrodynamically bound cell is equally likely $P_+ = 1/2$ to escape either to the left or right of its point of contact. Cells that approach the surface along the tangent collide at an angle well outside of the basin of attraction and rapidly escape while maintaining the direction of their tangential motion (i.e., $P_+ = 1$). Cells that strike at intermediate angles may diffuse into the basin of attraction before escaping.

Combining this hypothesis with the results of the previous section implies that the orientation $\theta = 0$ changes from an unstable orientation to a stable orientation as the cell approaches the wall. Notably, this bifurcation must be either a transcritical bifurcation or a pitchfork bifurcation [40]. The former of these options is excluded by the symmetry of the system, which requires that the angular velocity ω_{near} be an odd function of θ . A supercritical pitchfork bifurcation is similarly excluded as it predicts the existence of stable orientations of approaching cells far from the boundary, which is inconsistent with the wide distribution of incident angles [see Fig. 2(d)] and the measured angular velocity of cells [see Fig. 3(b)]. Thus, we expect that as the cell approaches the wall, the fixed point $\theta = 0$ undergoes a subcritical pitchfork bifurcation that stabilizes this orientation while generating unstable fixed points at $\pm\theta_b$.

This reasoning gives little insight into torques acting on a cell that is turned to large angle, where both hydrodynamic interactions and contact forces between hundreds of rotating flagella and the surface are likely important. In response to this uncertainty, we make the simple assumption that the angular velocity saturates to some maximum value of ω_{max} . It should be noted that the value ω_{max} likely reflects an average over hydrodynamic and contact forces [41].

To analyze the motion of cells in contact with a surface, we consider a minimal model that includes the normal form of a subcritical pitchfork bifurcation and predicts a bounded angular velocity. We propose

$$\omega_{\text{near}}(\theta) = \begin{cases} K \left[\left(\frac{\theta}{\theta_b} \right)^2 - 1 \right] \theta & |\theta| \leq \theta_c \\ \text{sgn}(\theta) \omega_{\text{max}} & |\theta| > \theta_c \end{cases} \quad (2)$$

where K is a rate coefficient and θ_c is the angle at which the angular velocity saturates to $\omega_{\text{max}} = K[(\theta_c/\theta_b)^2 - 1]\theta_c$.

To test this hypothesis, we map the escape of a cell from the wall onto a first passage problem. Our measurements provide the probability P_+ that a cell that strikes the surface at a particular angle θ_{in} escapes at an angle $\theta_{\text{out}} > 0$ within a time t . For a given choice of θ_b , K , ω_{max} , and rotational diffusion coefficient D_{rot} , we calculate the probability that a cell is rotated to an orientation $\theta = \pi/2$ (at which it escapes in the positive sense) before it is turned to an orientation $-\pi/2$. We calculate how this probability varies with the incident angle and find the distribution of first passage times. For sake of simplicity, we assume that D_{rot} does not vary during the time that the cell is in contact with the surface.

We solve this first passage problem by way of a Fokker-Planck equation. Let $p(\theta, t)$ be the probability density that the flagella of a cell exert a net force oriented at an angle θ off of the surface normal at time t . The probability distribution

evolves in time as

$$\frac{\partial p}{\partial t} = -\frac{\partial}{\partial \theta}(\omega_{\text{near}} p) + D_{\text{rot}} \frac{\partial^2 p}{\partial \theta^2}. \quad (3)$$

As cells rapidly escape into the bulk fluid when they are turned away from the boundary, we assume absorbing boundaries at $\theta = \pm\pi/2$. To solve this first passage problem for a given choice of model parameters, we first calculate the probability flux $j(\theta, t) = \omega_{\text{near}} p - D_{\text{rot}} \partial p / \partial \theta$ and find the fluxes j_- and j_+ to boundary left and right boundaries, respectively. The probability that a cell escapes in the positive sense at a time t is $P_+(t) = j_+ / (j_- + j_+)$.

We first consider the fate of a cell that strikes the boundary at an angle θ_{in} . The probability $P_+(\theta_{\text{in}})$ that the cell eventually escapes in the positive sense can be found from the Greens functions $p_g(\theta, \theta_{\text{in}})$ of Eq. (3) at steady state. It is convenient to normalize p_g such that $P_+ = -(\partial p_g / \partial \theta)_{\theta=\pi/2}$. These normalized Green's functions are solutions of

$$0 = -\frac{\partial}{\partial \theta}(\tilde{\omega}_{\text{near}} p_g) + \frac{\partial^2 p_g}{\partial \theta^2} + \delta(\theta - \theta_{\text{in}}), \quad (4)$$

where $p_g(\pm\pi/2, \theta_{\text{in}}) = 0$, $\delta(\theta)$ is the Dirac delta function, and $\tilde{\omega}_{\text{near}} = \omega_{\text{near}} / D_{\text{rot}}$ is the dimensionless angular velocity. It follows from Eq. (2) that $P_+(\theta_{\text{in}})$ depends on three dimensionless combinations of the four unknown model parameters D_{rot} , θ_b , K , and ω_{max} (or equivalently θ_c). These dimensionless model parameters can be expressed as the size θ_b of the basin of attraction of the stable orientation $\theta = 0$, the typical Brownian fluctuations $\sigma = \sqrt{D_{\text{rot}} / 2K}$ about this fixed point, and the ratio $\text{Pe} = \pi \omega_{\text{max}} / 2D_{\text{rot}}$ of maximum hydrodynamic and Brownian torques acting on escaping cells.

To compare this model to observation [see Fig. 4(a)] for a given choice of θ_b , σ , and Pe , we discretize the interval $-\pi/2 < \theta < \pi/2$ into 300 elements and numerically integrate Eq. (4) using standard finite element methods for linear equations [42] and calculate $P_+(\theta_{\text{in}})$ for 150 regularly spaced choices of $0 \leq \theta_{\text{in}} < \pi/2$. We fit θ_b , σ , and Pe by adjusting these parameters to match the results of the numeric integration of Eq. (4) and observation. The black line in Fig. 4(a) shows the least-squares fit to the observed dependence of escape direction on incident angle. We find $\theta_b = 15^\circ \pm 2^\circ$, $\sigma = 22^\circ \pm 5^\circ$, and $\text{Pe} = 5.7 \pm 2.5$. The reported uncertainties represent the 95% confidence interval in the parameter values found by a boot strap in which this fitting procedure is repeated 1000 times on randomly selected subsets of the observed collisions.

These fit values provide two points of physical insight into the motion of cells neat a surface. Because $\sigma > \theta_b$, the Brownian fluctuations in orientation are slightly greater than the basin of attraction of the hydrodynamically bound state. Thus, cells are only briefly localized near the surface. That $\text{Pe} = 5.7 \pm 2.5$ is somewhat greater than unity indicates that cells that collide with the surface outside the basin of attraction of $\theta = 0$ rarely become trapped.

Next, we consider how the probability that a cell escapes in the positive sense decays as it remains in contact with the surface, as shown in Fig. 4(c). Nondimensionalizing time in Eq. (3) by the diffusive timescale $\tau_D = \pi^2 / D_{\text{rot}}$ and solving relates the distribution incident angles to the fraction of cells $P_+(t/\tau_D)$ that escape in the positive sense for a given choice

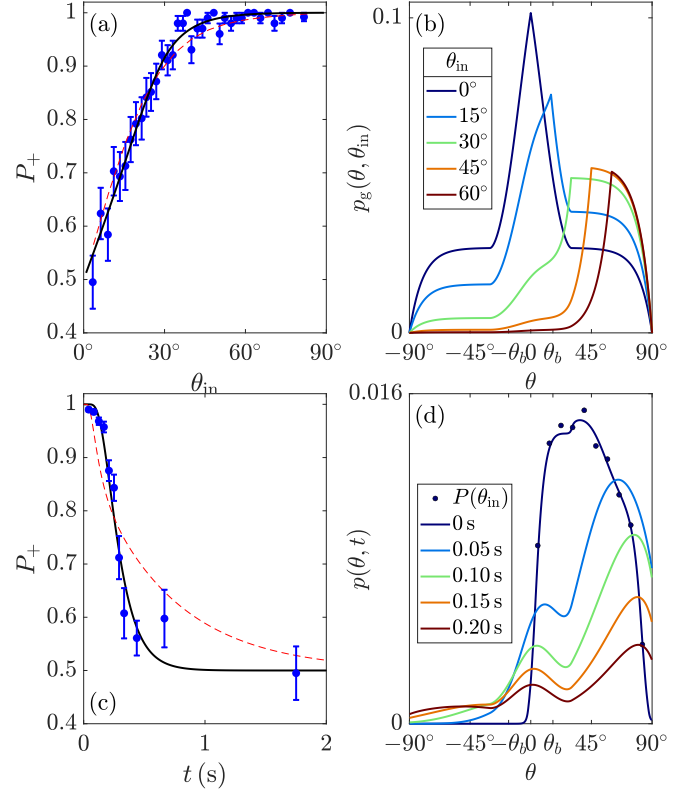


FIG. 4. Probability P_+ that a cell escapes the surface at an angle $\theta_{\text{out}} > 0$ is greatest for cells that collide at small angles or quickly escape. (a) P_+ is measured for several thousand collisions at a variety of incident angles θ_{in} . The black line shows the best fit to Eq. (4). The red dashed line shows the comparison to the null model in which cells are rotated according to Eq. (1) and the prefactor is fit. Error bars indicate the 95% confidence intervals. (b) The steady-state distribution of cells is shown with sources at several choices of θ_{in} . These distributions are normalized such that $j_+ + j_- = 1$. (c) Cells that escape the surface quickly escape at positive angles ($P_+ = 1$). Those that become trapped eventually escape with equal probability in either direction ($P_+ = 1/2$). The black line shows the best fit to the Fokker-Planck equation using the same parameters as in panel (a). These data are the same as in Fig. 1(f) but scaled linearly to better compare to the model. The null model (red dashed line), which uses the same parameters as in panel (a), poorly predicts the temporal evolution of P_+ . (d) Solutions of the Fokker-Planck equation are shown at five time points. The initial distribution is interpolated from the measured distribution of incident angles $P(\theta_{\text{in}})$.

of θ_b , σ , and Pe . Figure 4(d) shows how distribution of orientations evolve as cells escape from the surface and become trapped at $\theta = 0$. These solutions begin from the measured distribution of incident angles and use the parameter values fit to Fig. 4(a). These dynamics uniquely define the functional form of $P_+(t/\tau_D)$, where the diffusive timescale τ_D is the only unknown parameter. We fit τ_D by rescaling the measured decay of P_+ to the predicted functional form. We find $D_{\text{rot}} = 1.15 \pm 0.1 \text{ rad}^2/\text{s}$, which implies $K = 4.22 \pm 2.11 \text{ s}^{-1}$ and $\omega_{\text{max}} = 6.92 \pm 0.18 \text{ rad/s}$. These values correspond to a critical angle $\theta_c = 31^\circ \pm 2^\circ$ beyond which ω_{near} saturates to ω_{max} . Figure 2(c) compares the measured cumulative distribution function of escape times to the probability $\int_0^T j_+(t) + j_-(t) dt$

that a cell escapes before time T . Similarly, the escape entropy corresponding to the best fit of $P_+(t)$ is shown in Fig. 2(f).

The measured variations of P_+ with incident angle and time are inconsistent with the physical null model that the far-field hydrodynamic effect of a boundary can be extended to model the motion of a cell in contact with a surface. We repeat the procedure described above to fit P_+ to the Fokker-Planck equation where the drift velocity is described by Eq. (1) and the prefactor on the sinusoidal term is fit. As shown in Figs. 4(a) and 4(c), while the variation with incident angle is equally well described by either model, the first passage times differ markedly.

C. Matching near- and far-field dynamics

The agreement between theory and observation shown in Fig. 4 leads us to conclude that Eq. (2) captures the essential qualities of the near field dynamic coupling between a *T. majus* cell and a wall. Two questions remain. First, these results do not constrain the distance between a cell and the wall at which a cell may become trapped. Additionally, it is not clear why all cells escape the surface at narrowly distributed angles (see Fig. 2).

To answer these questions we match the short-range angular velocity [Eq. (2)] with the far-field [Eq. (1)]. To match the cubic decay of torques on the cell predicted by the far-field dynamics, we propose that at short distances $z \sim a$ from the wall and small angles ($\theta < \theta_c$)

$$\omega(z, \theta) = \frac{K\theta}{[(z-a)/\eta + 1]^4} \left[\left(\frac{\theta}{\theta_b} \right)^2 + \frac{z-a}{\eta} - 1 \right], \quad (5)$$

where η is the thickness of the gap between the cell and wall at which the orientation $\theta = 0$ becomes stable. In the limit $z \gg \eta$ and $\theta \ll \theta_b$, this expansion matches Eq. (1) where $\eta/a = (9\ell U/32Ka)^{1/3} = 1.27 \pm 0.16$. We conclude that cells may become bound when the gap between the cell and the wall becomes similar to the cell radius. This result is intuitively consistent with the physical model in Ref. [27], in which the bound state is stabilized because velocity gradients in the gap between cell and surface are sharper than those between the cell and the bulk fluid causing the cell to roll to align its flagella with the surface normal.

Finally, we consider the escape of a cell from the surface. All cells escape by first swimming tangent to the wall. We consider the simplest function that interpolates between the constant angular velocity ω_{\max} found when the cell is in contact with the surface the cubic decay predicted by the far field. We expect the angular velocity of an escaping cell to decay as

$$\omega(\theta, z) = \frac{\omega_{\max}}{[(z-a)/\eta + 1]^3}. \quad (6)$$

Cells escape with speed $dz/dt = -U \cos(\theta) + u_{\text{im}}(z, \theta)$, where $u_{\text{im}}(z, \theta)$ is a correction to the swimming speed due to advection by the cell's hydrodynamic image. Its functional form is provided in Ref. [36].

We numerically integrate Eq. (6) to find the asymptotic orientation of a cell's motion that is initially swimming tangent to the surface. Taking the initial distance between the cell and the wall to be one cell radius, we find—with no

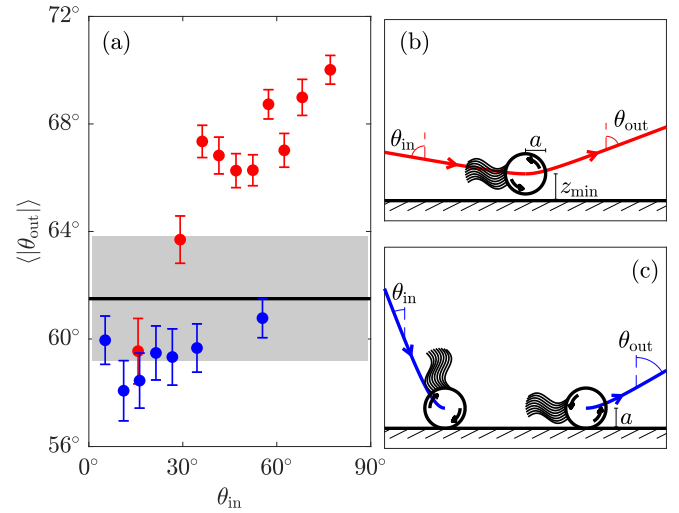


FIG. 5. The escape angle is determined by the minimum distance between the cell and the wall. (a) The average escape angles (blue dots) of cells that remain in contact for at least 0.125 s are similar with the prediction (black line with shaded 95% confidence intervals) of Eq. (6). Cells that remain in contact with the wall for shorter durations escape at slightly greater angles (red dots). The colors of these dots correspond to the conjectured trajectories shown in panels (b) and (c). Error bars indicate the 95% confidence intervals. (b) The red line shows the trajectory of a cell that approaches the surface at a shallow angle and is turned away from the surface before contact. It escapes from a height z_{\min} . (c) A cell that collides with the surface at a sharper angle eventually escapes from a height of a cell radius a . The blue line illustrates the approach and eventual escape of a cell that is briefly trapped.

fit parameters—a predicted escape angle of $61.5^\circ \pm 2.3^\circ$. As shown in Fig. 5, this value is consistent with the measured escape angle $\langle |\theta_{\text{out}}| \rangle = 59.5^\circ \pm 0.7^\circ$ found for cells that remain in contact with the surface for at least 0.125 s.

Curiously, cells that are identified by the tracking algorithm to be in contact with the surface for shorter durations escape at slightly greater angles, which increase with the incident angle (see Fig. 5). We believe that these events reflect the limit of the method that we adopted to identify collisions between a cell and the boundary. In the preceding analysis, we assume that a cell is in contact with the surface when its center comes within the measured cell radius of the boundary. The low spatial resolution of these measurements make this interpretation sensitive to diffraction. We believe that cells that fleetingly approach the surface (i.e., those that are identified by the algorithm to be in contact for less than 0.125 s) are turned away from the surface by hydrodynamic torques before they come in physical contact with the wall, similar to the scattering of *Chlamydomonas* [43]. Taking the minimum distance between the cell and the wall to be z_{\min} and integrating Eq. (6), we find that the observed increase in $\langle |\theta_{\text{out}}| \rangle$ is consistent with a value of z_{\min} that increases monotonically with θ_{in} .

IV. CONCLUSION

In conclusion, we have used the scattering statistics of collisions between *T. majus* and a hard wall to probe the

near-field dynamics between a fast-swimming multiflagellated cell and a surface. A simple physical picture emerges. As a cell approaches a wall, dipole-dipole interactions with its hydrodynamic image turn the cell to swim parallel to the surface. When the distance between the cell and the surface decreases to a value of ≈ 1.27 cell radii the torques acting on the cell change qualitatively. Shear forces in the gap between the cell and the surface orient the cell to exert a force normal to the surface. The cell becomes trapped. We find that the basin of attraction of the fixed point is narrow. Consequently, most cells collide with the surface outside of this basin and rapidly escape while maintaining their direction of motion tangent to the surface. When a cell is captured by the stable fixed point, its eventual escape is symmetric and all information of its approach to the wall is erased. Because all cells that come in contact with the surface escape by first swimming tangent to the wall at a distance of one cell radius, all cells escape at similar angles. A minority of cells are turned from the wall before coming in physical contact with the wall and escape at slightly greater angles.

The trapping of *T. majus* by a hard surface is the first step in the nucleation of active chiral crystals [26]. In our previous study, we found that isolated cells remain trapped by the surface for tens of seconds [27], much longer than average trapping time 0.21 s found here. We ascribe this difference to the roughness of the walls made of PDMS to those made of polished glass. As the gap between the cell and the surface is presumably much smaller if the surface is smooth, the velocity gradient between the cell and the wall—which stabilize the trapped cell—is much sharper. Consequently, we expect cells

are more strongly trapped by cover slips than microfluidic walls. The escape of cells could be further enhanced by the sporadic binding of quickly rotating flagella to the PDMS, which may increase the effective rotational diffusion of cells, causing cells to escape more quickly from PDMS than from glass. This result highlights the importance of an unnaturally smooth surface for the formation of active chiral crystals. We are consequently doubtful of the biological significance of this form of collective motion.

Nonetheless, the dynamics by which cells scatter from rough surfaces are likely quite important for the ecology of *T. majus*. These bacteria, which live in the pore space of water-saturated sand, exude mucus tethers from their posteriors to attach to detritus [20]. It is not understood how cells attach this mucus thread to a surface. Our results show that when a cell collides with a surface outside of a narrow basin of attraction, it rapidly escapes rather than swimming parallel to the surface. As free-swimming *T. majus* frequently drag short tethers as they swim [23] and collisions quickly turn the cell posterior toward the wall, it is plausible that these collisions facilitate attachment of the tether to the surface. Given a swimming speed of 600 $\mu\text{m/s}$ and a pore size of several tens of micron, these collision dynamics provide several opportunities a second for a dragged tether to stick to a surface.

ACKNOWLEDGMENTS

We thank D. Das and A. Kudrolli for their insightful comments and discussions. This work was supported by NSF Grant No. PHY-2042150.

-
- [1] M. Fletcher and D. C. Savage, *Bacterial Adhesion: Mechanisms and Physiological Significance* (Springer Science & Business Media, New York, 2013).
 - [2] R. M. Harshey, *Annu. Rev. Microbiol.* **57**, 249 (2003).
 - [3] F. Azam and R. A. Long, *Nature (London)* **414**, 495 (2001).
 - [4] M. S. Datta, E. Sliwerska, J. Gore, M. F. Polz, and O. X. Cordero, *Nat. Commun.* **7**, 11965 (2016).
 - [5] E. Lauga and T. Powers, *Rep. Prog. Phys.* **72**, 096601 (2009).
 - [6] D. Lopez and E. Lauga, *Phys. Fluids* **26**, 071902 (2014).
 - [7] A.-J. Buchner, K. Müller, J. Mehmood, and D. Tam, *Proc. Natl. Acad. Sci. USA* **118**, e2102095118 (2021).
 - [8] S. E. Spagnolie, G. R. Moreno-Flores, D. Bartolo, and E. Lauga, *Soft Matter* **11**, 3396 (2015).
 - [9] H. Chen and J.-L. Thiffeault, *J. Fluid Mech.* **916**, A15 (2021).
 - [10] W. M. Durham, O. Tranzer, A. Leombruni, and R. Stocker, *Phys. Fluids* **24**, 091107 (2012).
 - [11] K. Drescher, K. C. Leptos, I. Tuval, T. Ishikawa, T. J. Pedley, and R. E. Goldstein, *Phys. Rev. Lett.* **102**, 168101 (2009).
 - [12] F. D. Müller, D. Schüler, and D. Pfeiffer, *J. Bacteriol.* **202**, e00398 (2020).
 - [13] N. Waisbord, A. Dehkharghani, and J. S. Guasto, *Nat. Commun.* **12**, 5949 (2021).
 - [14] A. Petroff, A. Rosselli-Calderon, B. Roque, and P. Kumar, *Phys. Rev. Fluids* **7**, 053102 (2022).
 - [15] S. H. Zinder and M. Dworkin, in *The Prokaryotes*, 3rd ed., Vol. 1, edited by Martin Dworkin *et al.* (Springer, Heidelberg, 2006), p. 185.
 - [16] W. De Boer, J. La Rivière, and A. Houwink, *Antonie van Leeuwenhoek* **27**, 447 (1961).
 - [17] J. LaRivière, in *Symposium on Marine Microbiology* (Charles C. Thomas, Springfield, IL, 1963), pp. 61–72.
 - [18] C. Wirsén and H. Jannasch, *J. Bacteriol.* **136**, 765 (1978).
 - [19] I. P. Marshall, P. C. Blainey, A. M. Spormann, and S. R. Quake, *Appl. Environ. Microbiol.* **78**, 8555 (2012).
 - [20] H. Schulz and B. Jørgensen, *Annu. Rev. Microbiol.* **55**, 105 (2001).
 - [21] F. Garcia-Pichel, *J. Bacteriol.* **171**, 3560 (1989).
 - [22] R. Thar and M. Kühl, *Proc. Natl. Acad. Sci. USA* **100**, 5748 (2003).
 - [23] T. Fenchel and R. Glud, *Nature (London)* **394**, 367 (1998).
 - [24] R. Thar and M. Kühl, *Appl. Environ. Microbiol.* **68**, 6310 (2002).
 - [25] A. P. Petroff, A. L. Pasulka, N. Soplop, X.-L. Wu, and A. Libchaber, *R. Soc. Open Sci.* **2**, 150437 (2015).
 - [26] A. P. Petroff, X.-L. Wu, and A. Libchaber, *Phys. Rev. Lett.* **114**, 158102 (2015).
 - [27] A. Petroff and A. Libchaber, *New J. Phys.* **20**, 015007 (2018).
 - [28] D. Das and E. Lauga, *Phys. Rev. E* **100**, 043117 (2019).
 - [29] K. Ishimoto, *J. Fluid Mech.* **880**, 620 (2019).
 - [30] T. H. Tan, A. Mietke, J. Li, Y. Chen, H. Higinbotham, P. J. Foster, S. Gokhale, J. Dunkel, and N. Fakhri, *Nature (London)* **607**, 287 (2022).

- [31] See Supplemental Material at <http://link.aps.org/supplemental/10.1103/PhysRevE.109.034403> for two representative videos of collisions between a cell and a surface.
- [32] H. C. Berg, *Random Walks in Biology* (Princeton University Press, Princeton, NJ, 1993).
- [33] E. Q. Z. Moen, K. S. Olsen, J. Rønning, and L. Angheluta, *Phys. Rev. Res.* **4**, 043012 (2022).
- [34] B. Jørgensen and N. Revsbech, *Appl. Environ. Microbiol.* **45**, 1261 (1983).
- [35] G. M. Whitesides, E. Ostuni, S. Takayama, X. Jiang, and D. E. Ingber, *Annu. Rev. Biomed. Eng.* **3**, 335 (2001).
- [36] K. Drescher, J. Dunkel, L. H. Cisneros, S. Ganguly, and R. E. Goldstein, *Proc. Natl. Acad. Sci. USA* **108**, 10940 (2011).
- [37] J. Blake, in *Mathematical Proceedings of the Cambridge Philosophical Society*, Vol. 70 (Cambridge University Press, Cambridge, 1971), pp. 303–310.
- [38] R. Vogel and H. Stark, *Eur. Phys. J. E* **35**, 15 (2012).
- [39] M. Jabbarzadeh and H. C. Fu, *Phys. Rev. E* **97**, 012402 (2018).
- [40] S. H. Strogatz, *Nonlinear Dynamics and Chaos with Student Solutions Manual: With Applications to Physics, Biology, Chemistry, and Engineering* (CRC Press, Boca Raton, FL, 2018).
- [41] V. Kantsler, J. Dunkel, M. Polin, and R. E. Goldstein, *Proc. Natl. Acad. Sci. USA* **110**, 1187 (2013).
- [42] J. N. Reddy, *An Introduction to the Finite Element Method*, Vol. 3 (McGraw-Hill, New York, 2005).
- [43] E. Lushi, V. Kantsler, and R. E. Goldstein, *Phys. Rev. E* **96**, 023102 (2017).